SYNTHESIS OF GRAPHENE OXIDES DOPED MOLYBDENUM OXIDE THIN FILM BY SPRAY PYROLYSIS FOR CARRIER SELECTIVE CONTACT AND THEIR EFFECTS ON SILICON BASED SOLAR CELL PERFORMANCE

BASHIR YUSUF

UNIVERSITI SAINS MALAYSIA

2022

SYNTHESIS OF GRAPHENE OXIDES DOPED MOLYBDENUM OXIDE THIN FILM BY SPRAY PYROLYSIS FOR CARRIER SELECTIVE CONTACT AND THEIR EFFECTS ON SILICON BASED SOLAR CELL PERFORMANCE

by

BASHIR YUSUF

Thesis submitted in fulfilment of the requirements
for the degree of
Doctor of Philosophy

June 2022

DEDICATION

I dedicate this work to our first teacher, prophet Mohammad (Peace be upon him). I also dedicated the thesis to my mother, my father, and my children. May Allah make this work beneficial to the entire world.

ACKNOWLEDGEMENT

In the name of Allah, the Most Beneficent, the Most Merciful.

All praise and thanks are due to the **Almighty ALLAH SUBHANAHU WA TAALA,** the lord of the word, for giving me the health, strength, knowledge and patience to complete this thesis, words are not enough to bestow thanks and praise to the **Almighty ALLAH.**

I would like to express my deep gratitude to my main supervisor, Professor Dr. Md Roslan Hashim, Deputy Vice-Chancellor Sustainability and Institutional Development, Universiti Sains Malaysia (Professor in Nanotechnology, School of Physics, Universiti Sains Malaysia). Your contribution as a teacher, mentor and father have widened my horizon in conducting this research. I thank you, sir, for your guidance, support, and encouragement. Furthermore, my appreciation and gratitude go to my co-supervisors Dr Mohd Mahadi Halim and Dr Mohd Zamir Pakharuddin, for giving this thesis scientific input and support.

I would like to express my sincere gratitude and thanks to the School of Physics Staff. My acknowledgement also goes to the staff of NOR Lab for their help and guidance in conducting the synthesis fabrications and characterizations of the devices. Also, like to acknowledge all colleagues in NOR Lab, especially Nurizati and those whose names may have been missed to mention here for your help and support.

Last but not the least, I would like to express my truthful gratefulness to my beloved family who are always in my heart; my mother, wife, wonderful children Hakeem, Hafsat, Hafeez, and Zahara my brother Abdallah, and friends, Aminu, Munir, Dahiru, Likit, Habibu, Babangida and Musa Gaida.

Bashir Yusuf

Penang Malaysia, 2022

TABLE OF CONTENTS

LIST OF TABLES

Page

LIST OF FIGURES

Page

LIST OF SYMBOLS

α	Alpha functions
V	Applied voltage
T	Absolute temperature
K	Boltzmann constant
θ	Bragg's angle
ϕ_B	Barrier height
I	Current
D	Crystallite size
$℃$	Degree
q	Charge
A^{**}	Effective Richardson constant
μ_n	Electron mobility
e-h	Electron-hole
$h\nu$	Energy of photon
E_F	Fermi energy level
β	Full width at half maximum
η	Ideality factor
J_o	Saturation current density
ε	Strain
λ	Wavelength
A	Area
m^*	Effective mass
R_H	Hall coefficient
V_H	Hall Voltage
P_{in}	Incident solar power

I_m	Maximum current
P_m	Maximum power
h	Planck constant
R	Resistance
σ	Conductivity
ρ	Resistivity
R_{sh}	Shunt resistance
J_{SC}	Short circuit current density
Rs	Series resistance
(hkl)	Miller indices

LIST OF ABBREVIATION

rms	Root mean square
V_B	Valence band
I-V	Current-voltage
C_B	Conduction band
AFM	Atomic force microscope
MoO_3	Molybdenum triodes
NH_4OH	Ammonium hydroxide
H_2O_2	Hydrogen peroxide
EDX	Energy-Dispersive X-ray spectroscopy
FESEM	Field Effect Scanning Electron Microscope.
XRD	X-ray diffraction
NBs	Nano belts
NWs	Nanowires
1*D*	1 Dimension
2*D*	2 Dimension
3*D*	3 Dimension
SPT	Spray Pyrolysis Technique
SiO_2	Silicon oxides
SiNx	Silicon Nitrides
RF	Radio Frequency
RCA	Radio Corporation of America
WO_3	Tungsten oxide
V_2O_5	Vanadium trioxides

SINTESIS FILEM NIPIS MOLIBDENUM OKSIDA TERDOP GRAFIN OKSIDA OLEH TEKNIK SEMBURAN PIROLISIS UNTUK SENTUHAN PEMBAWA TERPILIH DAN KESAN KE ATAS PRESTASI SEL SURIA BERASASKAN SILIKON

ABSTRAK

Fenomena lapisan pengangkutan pembawa terpilih telah berjaya digunakan selama tiga dekad yang lalu untuk sel solar hetero-simpang organik. Baru-baru ini, proses tersebut telah dipindahkan ke sel berasaskan silikon untuk mencapai fungsi yang sama. Teknik penyejatan termal telah digunakan untuk pemendapan filem. Walau bagaimanapun, keupayaan untuk mengawal kecacatan kekosongan oksigen melalui penyejatan termal adalah terhad dan keperluan untuk suhu pemendapan menghalang proses peningkatan kepada pengeluaran besar-besaran industri. Penyelidikan ini mengkaji pertumbuhan dan pencirian struktur nano molibdenum oksida (MoO_3) terdop grafin oksida dengan teknik pirolisis semburan untuk aplikasi pengangkutan pembawa selektif. Pada peringkat pertama, pengaruh keadaan pemendapan (larutan pH, molariti prekursor dan kadar aliran larutan) terhadap pertumbuhan dan sifat fizikal filem MoO_3 dianalisis. Hasil struktur menunjukkan pembentukan pertumbuhan lamela ortorombik sepanjang (0k0) untuk semua keadaan pemendapan. kesan medan (FESEM) mengesahkan pH, molariti, dan pergantungan kadar aliran larutan pada pembentukan geometri berlapis seperti tali pinggang nano. Analisis spektrum EDX mengesahkan kehadiran O, Mo, dan Si untuk semua keadaan pertumbuhan. Dari pengukuran voltan arus, ketinggian penghalang (Φ_B) dan faktor idealiti (n) mempunyai pergantungan yang kuat pada semua keadaan pemendapan. Pada peringkat kedua, pengaruh kepekatan pendopan GO pada sifat filem MoO_3 dikaji. Sifat fizikal filem MoO_3 terdop GO meningkat dengan ketara dibawah kepekatan

pendopan 2%, yang menunjukkan sebagai pendopan yang terbaik untuk aplikasi sentuhan pembawa terpilih kerana memberikan nisbah pengayaan tertinggi. Kemudian sel suria berdasarkan pertumbuhan filem MoO_3 GO yang didop pada keadaan yang dioptimumkan dibuat dan dicirikan. Sel suria terbaik menunjukkan kecekapan penukaran tertinggi 2.87%, V_{oc} 518.68 mV, J_{sc} 9.22 (mA/cm^2) dan FF 58.09%. Kepekatan Hall, kelincahan lohong dan kerintangan peranti didapati masing-masing $7.41\times10^{19}(cm^{-3})$, 2.68 ($cm^2V^{-1}S^{-1}$), dan 40.16 (Ωcm) Akhirnya, kestabilan prestasi peranti buatan yang disimpan selama tiga bulan di persekitaran terbuka dinilai. Diperhatikan bahawa peranti MoO_3 terdop GO dengan kepekatan 3%GO mengekalkan prestasi tertinggi setelah tiga bulan. Jsc, FF, dan η menurun secara mendadak untuk kepekatan 0%GO sehubungan dengan masa penyimpanan. Sementara itu, untuk pendopan 1% hingga 2% sedikit menurun.

SYNTHESIS OF GRAPHENE OXIDES DOPED MOLYBDENUM OXIDE THIN FILM BY SPRAY PYROLYSIS FOR CARRIER SELECTIVE CONTACT AND THEIR EFFECTS ON SILICON BASED SOLAR CELL PERFORMANCE

ABSTRACT

The carrier selective transport layer phenomenon has been successfully employed for organic heterojunction solar cells during the past three decades. Recently, the process has been transferred to silicon-based cells to achieve the same functions. The thermal evaporation technique has been used for film deposition. However, the ability to control the oxygen vacancy defect via thermal evaporation is limited, and the requirement for the deposition temperature obstructs the upscaling process to industrial mass production. This research examines the growth and characterizations of molybdenum oxide doped with graphene oxides nanostructures by spray pyrolysis technique for carrier selective transport applications. At the first stage, the influence of deposition conditions (pH solution, precursor molarity and solution flow rate) on the growth and physical properties of the MoO_3 films were analyzed. The structural results showed the formation of orthorhombic lamellar growth along (0k0) orientation for all the deposition conditions. The field emission scanning electron microscopes (FESEM) confirmed pH, molarity, and solution flow rate dependence on the formation of nanobelt-like layered geometry. The EDX spectrum analysis justified the presence of O, Mo, and Si for all the growth conditions. From the current-voltage measurements, the barrier height (Φ_B) and ideality factor (n) has a strong dependency on all the deposition conditions. At the second stage, the influence of GO doping concentrations on the MoO_3 film properties was examined. The physical properties of the GO-doped MoO_3 films were significantly improved under 2 % doping

concentration, which suggests the best doping for carrier selective contact application as it gives the highest rectification ratio. Then, the solar cells based on GO-doped MoO_3 films growth at optimized conditions were fabricated and characterized. The best solar cell exhibited the highest conversion efficiency of 2.87 %, V_{oc} of 518.68 mV, J_{sc} of 9.22 (mA/cm^2) and FF of 58.09 %. The Hall concentration, hole mobility and resistivity of the best-performing devices were also found to be 7.41×10^{19} (cm^{-3}), 6.21 ($cm^2V^{-1}S^{-1}$), and 40.16 (Ωcm), respectively. Finally, the performance stability of the fabricated devices stored for three months in an open environment was evaluated. It was observed that the MoO_3 doped with GO device at a 3 % doping concentration retained the highest performance after three months. The Jsc, FF, and η decrease tremendously for 0 % GO doping concentration with respect to storing time. Meanwhile, the Jsc, FF, and η for 1 % to 2 % doping content slightly decreases.

CHAPTER 1

INTRODUCTION

1.1 Introduction

The carrier selective transport layer phenomenon is one of the crucial aspects for improving solar cell devices [1]. The process has been successfully working during the past three decades to improve organic heterojunctions devices [2]. However, the process has been recently transferred to silicon-based devices to achieve the same function. The phenomenon will specifically ease in building large-area silicon-based heterojunction devices (SHJ) for solar cells application. The selective transportation of the holes and congruent block of electrons to an external circuit is mainly characterized by the band bent device segments close to the external metal electrodes. These segments form selective hole contacts at the heterointerface [3]. The barrier height at the segment for the carrier to be blocked must be higher, while the other barrier for which the contact is intended to be selected should be lower. The process will ease the carrier transport to external electrodes.

The future of silicon heterojunction (SHJ) devices is incredibly positive. The recent world's highest-performing device efficiency was achieved using the process. In typical SHJ, the hole conductions are attained by combining B-doped a-Si:H(p) film using c-Si technologies. The arrangements are usually considered as heterojunction with an intrinsic thin coating (HIT). However, the surface absorption of the c-Si were severely reduced due to the small optical bandgap (1.6–1.8 eV) and substantial B-doping of the B-doped a-Si:H(p) film. Therefore, several wide bandgap materials, like hydrogenated amorphous silicon carbide (a-SiCx:H) or hydrogenated amorphous silicon oxide (a-SiOx:H), were proposed to overcome the problem [4]. Moreover,

despite the enhance characteristics of (a-SiOx:H) or (a-SiCx:H), the carrier extraction to the maximum level was still hampered by low electrical performance and large band offsets at the a-Si/c-Si interface of SiOx [5]. Herein, 2D Transition Metal Oxides (TMOs), like molybdenum oxide (MoOx), with oxygen vacancies are of interest due to the presence of energy states close to the fermi level. The energy state could efficiently transport the hole to the external circuit and reduce recombination on the device interface [6].

Currently, several scientists are engaged in using MoO_3 for various engineering applications. It is an n-type semiconductor with excellent chemical properties, thermal consistency, direct optical band gap, and exceptional specific energy [7]. Due to these superior characteristics, many molybdenum nanostructures, such as; nanobelts [8], nanorods [9] and nanowires [10], have acquired collective attention among various researchers. Different techniques have been employed to prepare MoO_3 nanostructures on several types of substrate, among which includes sputtering [11], chemical vapour deposition [12], electro-deposition [13], microwave-assisted method [14], and spray pyrolysis [15]. Spray pyrolysis is comparatively simple and effective for large area deposition with good homogeneity and control over the processing parameters.

However, the improvement of molybdenum-based electronic devices has been strictly hindered by the lack of proper dopants for generating charge carriers. Although significant progress has been made in recent decades. These led to an extensive research of doping MoO_3 films with several metals such as tin (Sn) [16], indium (In) [17], bismuth (Bi) [18], iron (Fe) [19] and certain metal oxides like titanium oxide (TiO_2) [20, 21], vanadium oxide (V_2O_5) [22], manganese oxide (Mn_2O_3) [23], tungsten oxide (WO_3) [24], iridium oxide (Ir_2O_3) [25], zinc oxide (ZnO) [26], and graphene oxides (GO) [27]. Among all these dopant materials, oxygenated graphene called

graphene oxide, which contains many oxygens functional groups like ketone, carboxyl, epoxy, and hydroxyl at their basal and edge planes, offers a platform with a large surface area for decorating foreign atoms into the MoO_3 matrix. To the best of our knowledge, there are no records of a spray pyrolysis-based synthesis, which gives a clear understanding of physical properties of spray pyrolyzed MoO_3 and MoO_3 doped with GO thin films as carrier selective layers on silicon-based heterojunction for solar cells application.

1.2 Motivation and Problem Statement

MoO_3 is among other 2D transition metal oxides (TMOs) that have attracted significant interest worldwide owing to its remarkable properties for selective carrier applications [28, 29]. These properties led to numerous efforts to prepare the material films by various methods such as atomic layer deposition [30], sputtering [31], hot wire oxidation-sublimation [32], microwave-assisted method [33], thermal evaporation [7], and spray pyrolysis [15]. Spray pyrolysis has remained the most acceptable method for all these techniques due to its simplicity and possible large-surface deposition. Similarly, the methods can deposit high quality, uniform, and well-crystalline film in a short period. Furthermore, the film composition and stoichiometry can be controlled by doping and changing the spray parameters.

Silicon substrate has revealed numerous benefits compare with other substrates, and this benefit includes low cost and possible incorporation of typical Si-based optoelectronic devices. The growth of MoO_3 nanostructure on the Si-based substrate for hall carrier selective contact applications has gained considerable motivation. However, the spray pyrolysis method has not been extensively used to grow MoO_3 doped GO nanostructures on silicon substrate for carrier selectivity on

silicon based solar cells. The only recently reported molybdenum oxides hybrids PEDOT: PSS solar cells fabricated using spray pyrolysis yielded a lower efficiency of 5.11 %. Consequently, enormous efforts are needed to study the growth and physical properties of MoO_3 nanostructures for hall selective application, which is added to the understanding of their crystalline quality, morphological structure, doping nature, and selective carrier properties for photovoltaic applications**.**

1.3 Research Objectives

1. To ascertain the best growth parameters (solution pH, solution molarity and solution flow rate) that control the morphological, physical, and electrical properties of molybdenum oxides (MoO_3) thin film as selective hole contact by spray pyrolysis techniques.

2. To examine the impact of graphene oxides doping concentration on molybdenum oxides thin films properties for hole selective contact application.

3. To evaluate the silicon-based solar cell's performance and stability incorporating molybdenum oxide doped with graphene oxides thin film as an efficient hole selective contact.

1.4 The Originality of the Research

The originality of the thesis includes the following points:

1. Synthesis of MoO_3 thin film by spray pyrolysis technique with good crystallinity quality and electrical properties suitable for carrier selective contact devices.

2. Development of molybdenum doped with GO thin film on Si substrate by spray pyrolysis method for carrier selective contact application.

3. Fabrication of Si- based solar cells based on MoO_3 doped with GO thin-film solar cells on the silicon-based substrate.

4. Determination of the performance stability of pure and MoO_3 doped with GO thin-film solar cells as an efficient hole selective contact.

1.5 Thesis Outlines

The thesis consists of seven chapters, an introduction to molybdenum trioxides thin film for photovoltaic applications. The improvement of molybdenum-based electronic devices by doping process was presented in chapter 1. The chapter also includes the motivation, objective, original contribution and finally, the thesis outlines. Chapter 2 consists of theoretical background and literature review. The fundamental properties of molybdenum oxides films, the growth mechanism of molybdenum oxides films using various methods, the theoretical concept of solar cells and the evaluation of solar cells performance based on molybdenum oxides films was provided in the chapter. Chapter 3 described the methodology, equipment and instruments used in the experimental implementation. Chapter 4 presents the preliminary results that give the background of the research. This includes determining optimal growth parameters (solution pH, solution molarity and solution flow rate) of MoO_3 nanostructure using spray pyrolysis. The morphological, structural and electrical characterizations of the prepared films was also presented. In chapter 5, an explanation of the doping process of the MoO_3 doped with GO and characterizations of the prepared films were presented. Chapter 6 discussed the fabrication process of the silicon-based solar cell.

Chapter 7 summarizes the findings, conclusions, recommendations for future work and the research contributions.

CHAPTER 2

THEORETICAL BACKGROUND AND LITERATURE REVIEW

2.1 Introduction

This section presents the fundamental properties of MoO_3, the growth mechanism of thin films, and the theoretical background involving thin-film solar cells. The chapter starts with the essential properties of the MoO_3. The crystal structure, optical and electrical properties of the material are briefly described. The growth mechanism of thin film by various techniques was explained. The theoretical concept of solar cells, performances factors (open-circuit voltage, short circuit current, fill factor, performance efficiency) are clarified. Finally, the assessment of MoO_3 thin film processed by various techniques and solar cells characteristics behaviour of the material is summarized.

2.2 Fundamental Properties of MoO_3

Molybdenum trioxide (MoO_3) is among the transition metal oxides (TMOs) that has drawn considerable attention globally [34]. This is due to its incredible properties, such as nontoxicity [35], exceptional chemical stability [36], high transparency, and electrical and optical favorability [37]. Table 2.1 shows some fundamental properties of MoO_3.

Table 2.1: Fundamental properties of MoO_3 [37]

Properties of MoO_3	**values**
Lattice parameter	a = 1.4020 nm, b = 0.3703 nm, c = 0.3966 nm
Density	4.70 g/cm^3
Melting point	795 ºC
Stable crystal structure	orthorhombic
Bandgap	>3 eV

2.2.1 Nanostructures

Nanotechnology and nanoscience are often attracted significant attention since the previous years and serve as a leading area in developing a new application [38]. The arrangement of building blocks in nanostructure defines the properties of materials [39]. The properties of bulk materials are entirely different from nanomaterials. The nanostructures might be categorized as zero dimension (0D), e.g., (nanoparticles and quantum dot). The one dimension (1D), e.g., (nanorods, nanowires, nanoneedles and nanotubes). The two dimensions (2D), e.g., (nanoflake, nanosheet, and nano leave). The three dimensions (3D), e.g, (nanosphere and tetrapod) [40]. The dimension and scopes of nanomaterials are crucial factors in determining their characteristics properties. The materials nanoscale dimension gives a considerable change in physical, electrical, and chemical properties compared to the bulk material [41]. The variations in size have been found to result in some primary effects, which leads to surface nature and sizable characteristics [42]. First, the length-diameter fraction involves a rise in the surface-to-volume proportional changes. This, in turn, results in an improvement in the number of surface atoms. Secondly, quantum confinement can occur once the atom dimension is altered to a certain level [43].

2.2.2 Structural Properties

Molybdenum oxides can be found in several crystal variations [44], steady orthorhombic(α-MoO_3) [45], hexagonal (*h*-MoO_3) [46], and meta-stable monoclinic(*β*-MoO_3) [47], which all influence their applications. Though, the α-MoO_3 structure is more stable compare to others [48]. It is formed by a unit cell with an orthorhombic pattern [49], which consist of lamellar assembly having layers parallel to [010] direction [50]. The sheet arrangement is such that each sheet is attached to two sub-layers along with a corner-sharing plane of (100) and an edge-sharing zigzag plane at (001) [51]. The properties of the bonds among the adjacent and the parallel plane also differ. The plane along [010] are of van der Waals types, while along [100] and [001] are covalent and ionic, separately [50]. The van der Waals type associated with this 2-D material is an essential tool for carrier selective contact properties, because it allows the accommodation of defects and/or intercalation of atoms within the structure.

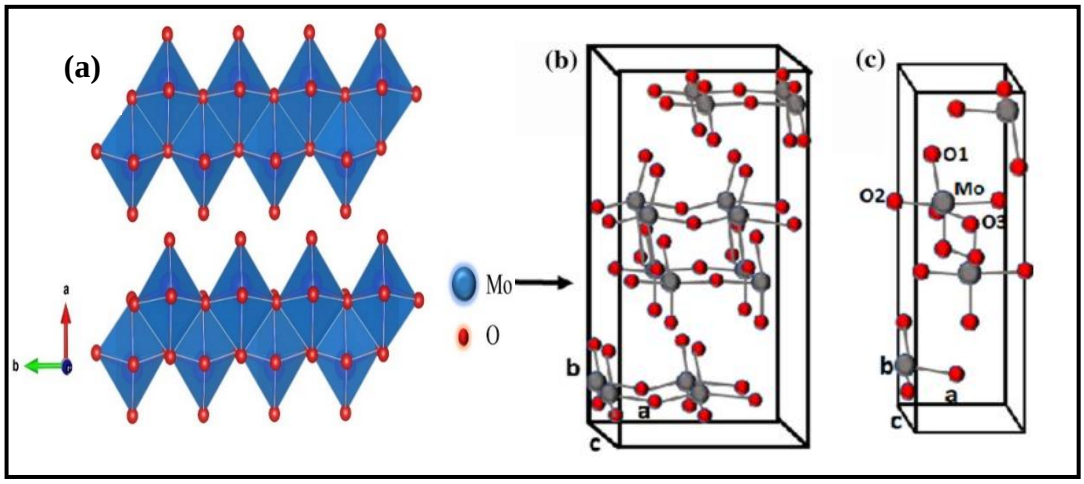

Figure 2.1: (a) MoO_3 crystal structure, (b) molecular bonding of MoO_3 crystal structure, (c) unit cell [52]

Fig. 2.1 (a) shows the orthorhombic MoO_3 crystal layered structures [53]. It consists of two networks of the corner-sharing octahedra MoO_6 associated with the sharing edges of 'a' and 'c' planes, i.e., (100) and (00l) planes, and weaker van der Waals along ' b' axis, i.e., (0k0) plane. The pictorial atomic arrangements are presented in Fig. (2.1 (b)). Moreover, Fig. (2.1 (c)) displays the three different oxygen sites: The oxygen O_2 is doubly attracted and joined with the two neighbouring atoms of Mo. While the terminal oxygen O_1 has a single bond to only Mo atom. Similarly, the O_3 is triply bonded with two Mo atoms along the c-axis [54].

2.3 Growth Mechanism of Thin Film Using Various Methods

Fig. 2.2 depicts the three basic categories of the film deposition process. The categorization was performed according to the physical, chemical, and solution-based processes. The physical type consists of molecular beam epitaxy [55], magnetron sputtering [56], pulsed laser deposition [57], and physical vapour deposition (PVD) [58]. Furthermore, electron beam evaporation [59] and chemical bath deposition [60] can be added. While the chemical categories comprise atomic layer epitaxy [61], atomic layer deposition (ALD) [62], and chemical vapour deposition (CVD) [63]. Meanwhile the solution based includes dip-coating [64], spin coating [65], sol-gel [66], and spray pyrolysis [67]. The three main identified distinct growth processes primarily depend on the growth conditions and materials device installation. For example, physical and chemical vapour depositions require a high cost of installation materials and specific deposition conditions. At the same time, the solution based can be fabricated and deposited at relatively easy techniques.

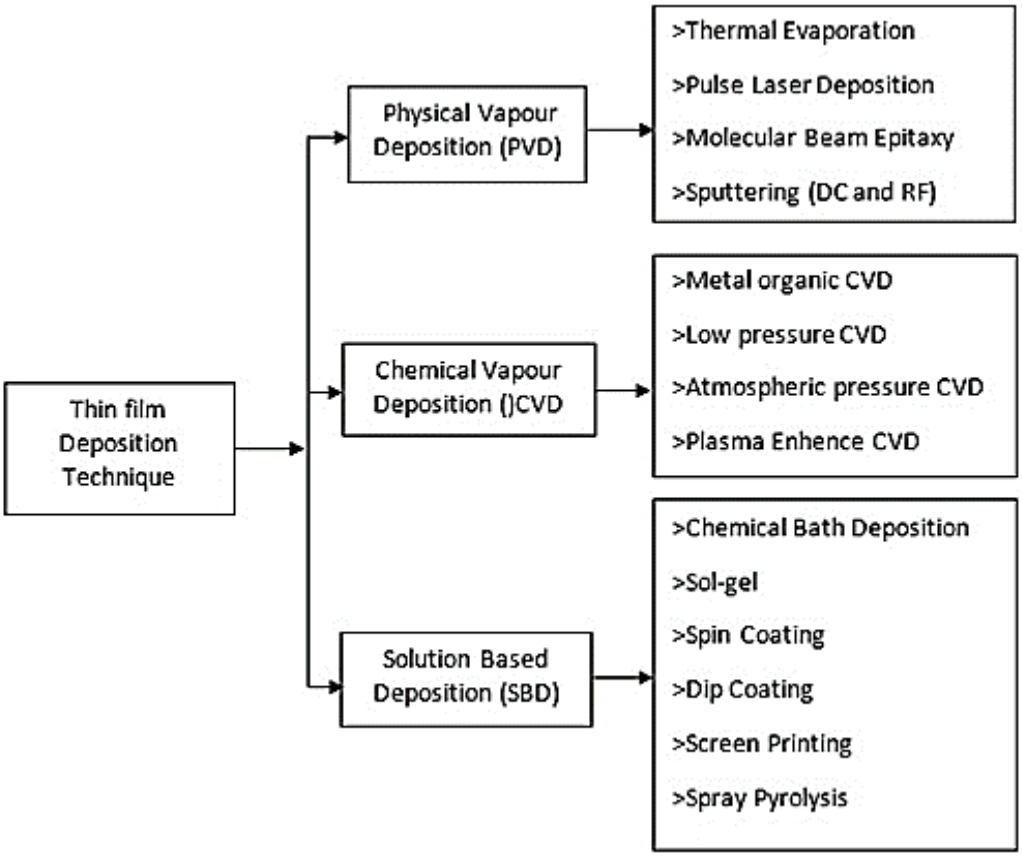

Figure 2.2: Classification of Thin-film Deposition Technique [68]

2.3.1 Spray Pyrolysis

Spray pyrolysis (SP) is a solution-based method for thin film deposition. In this method, the solution droplets of the material are produced by carrier gas at an elevated substrate temperature, thereby making the solution to be evaporated while the material solute decomposed into particles or nanofilm [69]. The techniques have some advantages, including simplicity, cost-effectiveness, and the possibility of a sizable surface area [70]. The average size of the droplets is generally small of about 20 μm. The approach is an adjustable processing mechanism for forming single and or multi-coated layers, porous and dense thin films [71]. The spraying types can be classified by considering the nature of the energy, which consists of; (1) tubular reactor, (2)

vapour flame reactor, (3) the emulsion combustion reactor and, (4) the flame spray pyrolysis system [72]. Similarly, spray type can be categorized according to atomization processes. This comprises; ultrasonic, electrostatic, and air-pressurized spray techniques [73]. The ultrasonic atomization works under an electromechanical device oscillating at an elevated frequency [74]. The Newtonian fluids with low viscosities allow the atomization to go through the oscillating surface. This oscillation originates the precursor to be atomized into a tiny droplet. In contrast, electrostatic spray involves using electric fields to attract the particles of atomized material onto the substrate [75]. A control voltage is usually applied between the substrate and nozzle, which generates sizable droplets at the nozzle end. Meanwhile, an air-pressurized spray pyrolysis process was adopted in this research. Moreover, the film structure could be modified by altering the solutions composites [76]. Various solvents can generate the solution composites, specifically chlorides, nitrates, and acetates, that can easily dissolve in an aqueous solvent. Other variables like; the precursor concentration [77], the solvent type [78], the carrier gas ratio [79], the distance between the substrate and nozzle [80], and the solution flow rate [81], could also be controlled. One major vital role of this method in relation to vapour-phase is the ability to control the film properties with exact desired stoichiometry.

2.3.2 Effect of Spray Parameters

It has remained a well-known phenomenon and experimentally proved in the literature that particle morphology can be modified by controlling the spray parameters [82]. The substrate temperature is one of the parameters that altered the properties of the sprayed films [83]. The substrate temperature also regulates the texture, crystallinity, and other properties of the film. Spraying at elevated substrate

temperatures produces porous film, while low substrate temperatures develop fractured films [84]. Another parameter that affects explicitly the films physical properties is precursor molarity [85]. However, the process of films formation by reaction kinetic can be explained in four developmental stages [86]. Stage A involves residing the droplets on the substrate before the solvent vaporizes. Stage B, the solvent immediately evaporates just before the droplet interacts with the substrate. Stage C is identified as the actual CVD process; as the droplet goes close to the substrate, the solvents evaporate. At this point, the solute dissolves and vaporizes. Subsequently, the vapour disperses and decomposes on the substrate surface to produce the desired thin film. Stage D is in vapour form the solute reaches the substrate in form of vapor. A comprehensive pictorial explanation of all the stages is shown in Fig 2.3 ((a) and (b)) and are marked as stages A, B, C and D, respectively.

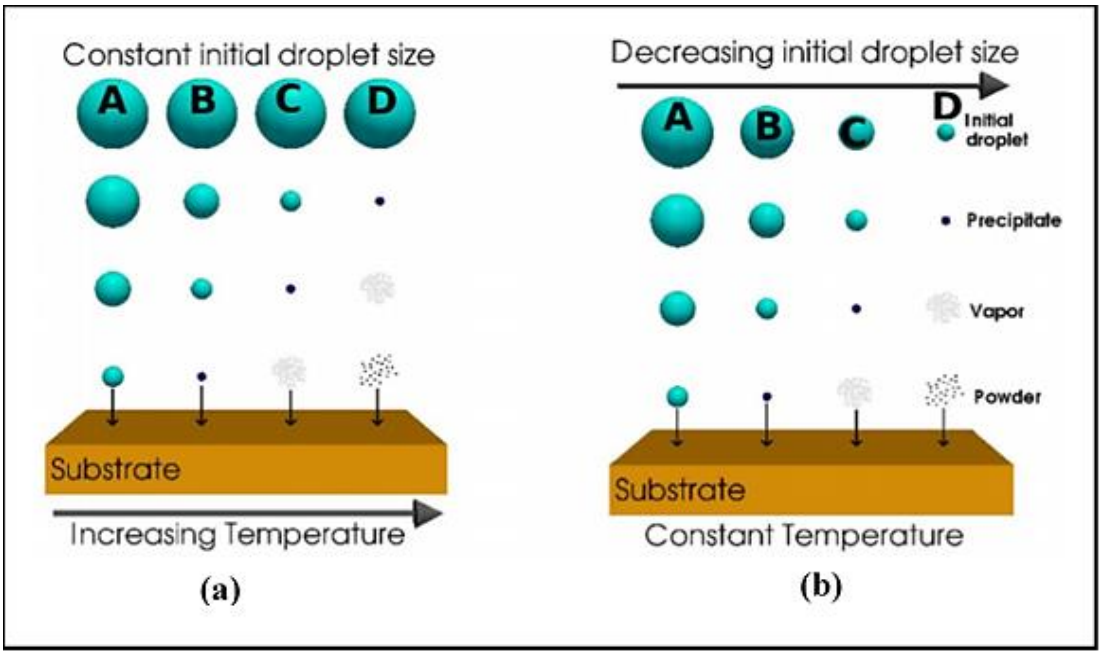

Figure 2.3: (a) increasing temperature at constant initial droplet (b) increasing initial droplet at a constant temperature [68]

2.4 The Theoretical Concept of Solar Cells

The solar cell theory gives the detailed procedure through which photons of light are transformed into electric currents. The conversion occurs when the photons strike an appropriate material. The theoretical justifications are of fundamental significance since they give the essential parameters of solar cells and explain the processes that lead to losses in the cell device.

2.4.1 Photogeneration of Charge Carriers

When photons strike the semiconducting material, their energies are transferred to the crystal lattice electron of the material. This electron is normally situated at the valance band of the semiconductor. The photons then give their energy to the material electron, which then moves the electron to the conduction band through which it can be moved freely in the semiconductor [87]. The freely removed electron will then create a vacancy called a hole [88]. A lost covalent electron makes the bonded electrons at nearby atoms migrate into the hole position. The phenomenon creates another hole, and this makes the hole to be moving throughout the lattice. Therefore, when photons strike the semiconductors, the electrons are excited and move from valence to conduction band [89]. However, for this phenomenon to occur, this photon energy must be greater than the semiconductor bandgap energy. Meanwhile, when the solar spectrum has photon energy greater than the semiconductor energy bandgap, the energy difference is normally transformed into heat by a process called lattice vibration [90].

2.4.2 The p-n Junction

The frequently used solar cell is designed based on the p-n junction on silicon-based devices. For an imagination, one might picture the creation of a p-n junction by direct contact of n-type with p-type. Practically, the silicon-based p-n junctions are not constructed in this format. However, the process involves doping n-type into the p-type wafer (or vice versa) [91]. Suppose a section of silicon p-type is placed in a nearby n-type. Consequently, the diffusion of electrons will happen from the part of more electrons (n-type) into the less electron part (p-type). The holes combine with electrons on the p-type portion at the p-n junction during the diffusion. However, when no external circuit is connected, the diffusion of these carriers does not continuously occur since the electric field produces charges on the other side. The produced electric field makes the charges transmit in a phenomenon called drift current [92]. The area where the two carriers move through the junction is known as the depletion region. The area comprises almost no mobile carriers. It is sometimes called the space charge region. The two forces (electric field and drift current) could oppose each other at every cell point. For example, the movement of the electrons across the junction is attributed to an electric field, which opposed the gradient concentration of the material. The same goes for the hole propagates in the reverse direction. The mechanism of charge carrier separation is through built in electric field. To avoid free carrier recombination, the diffusion length of minority carriers must be greater than the cell thickness. In amorphous silicon solar cells, the diffusion length of minority carriers is generally very small owing to silicon defects. Fig. 2.4 shows the schematic diagram of the process [93].

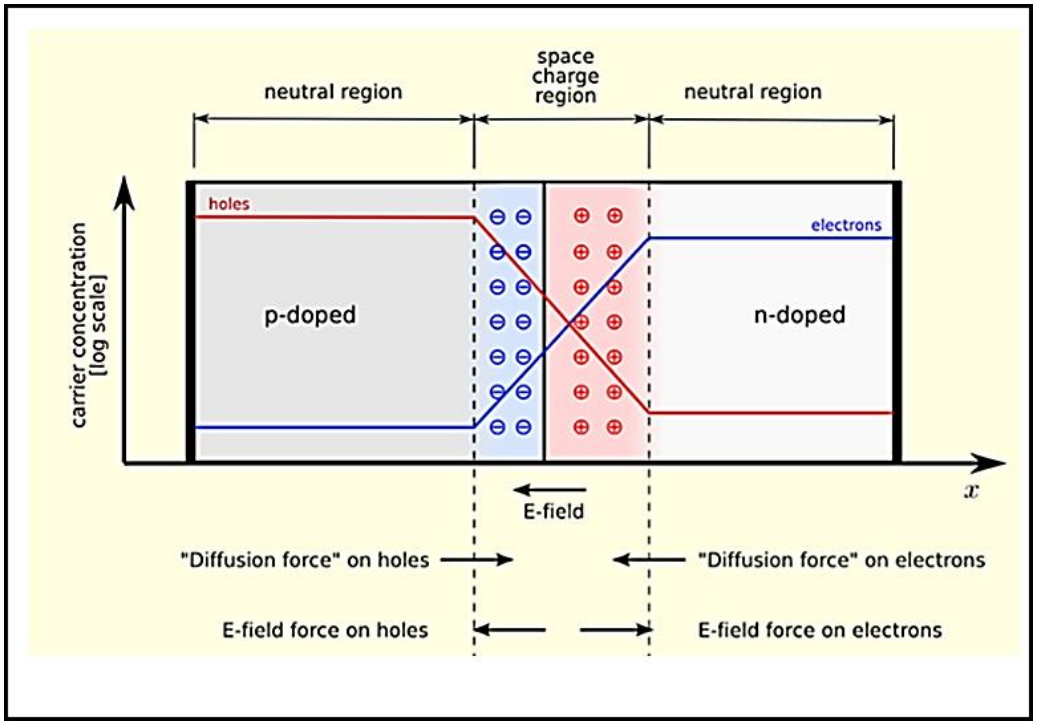

Figure 2.4: p-n junction diode in thermal equilibrium with zero bias voltage [94]

2.4.3 Performance Parameters of Solar Cell

Four fundamental factors estimate the solar cell performances; open-circuit voltage (V_{OC}), short-circuit current (I_{SC}), PCE, and fill factor (FF) [95]. Under light incidence, the path of current movement is from n-side to p-type. The produced electric charge in this process is referred to as light generated current (LC). At the open-circuit condition, where no external link between the n-type and p-type areas is made, the photogenerated current and thermally produced carriers must be well-adjusted by the reverse recombination current. The generated current rises as the potential barrier between the depletion section depressed. The formed potential barrier between the junction is generally called an open-circuit voltage Voc [96]. A significantly large V_{oc} could result in the reduction of the carrier recombination and hence improve charge collection efficiency [97]. Thus, it is critical to use an electrically correspondent

classical theory to understand the solar cell electronic properties. Experimentally, no ideal solar cell is possible. However, the two resistance components, series and shunt resistance, are involved for a proper explanation. The corresponding circuit of the cell is presented in Fig 2.5.

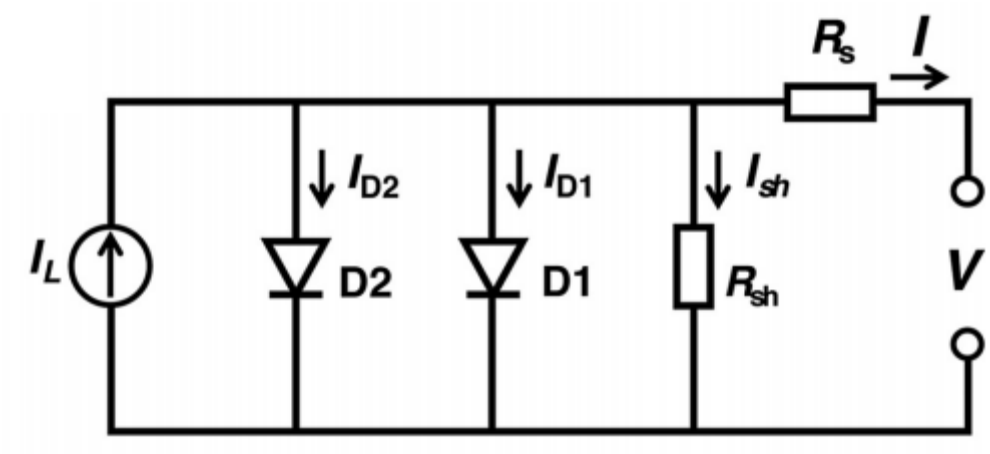

Figure 2.5: Equivalent circuit of practical solar cells [98]

Based on the corresponding circuit, it can be noticed that the produced current (I) is the same as the one produced by the current source, minus that of drifts current, minus current over the shunt resistor.

$$I = I_L - I_D - I_{SH} \quad 2.1$$

Where,

- I is the output yield current
- I_L is the photogenerated current (ampere)
- I_D is the current through the diode (ampere)
- I_{SH} is the shunt current (ampere).

The voltage across these resistors is,

$$V_j = V + IR_s \quad 2.2$$

where

- V_j is the diode and resistors voltages $R_{S.H}$ (volt)
- V is the output terminals voltages (volt)
- I is the output current (ampere)
- R_s is the diode series resistance (Ω).

Using the Shockley diode relation, the current over the diode will be,

$$I_D = I_O \left\{ \exp\left[\frac{V_j}{nV_T}\right] - 1 \right\} \quad 2.3$$

Where,

- I_o is the reverse saturation current (ampere)
- n is the diode ideality factor (which is 1 for an ideal diode)
- q is an electronic charge.
- k is Boltzmann's constant.
- T is an absolute temperature.
- $V_T = \frac{kT}{q}$ at T= 25 ºC, $V_T \approx 0.0259$ volt
- Where V_T threshold voltage (the gate voltage which form an inversion layer at the interface of insulating layer (oxide) and the substrate)

Using Ohms law, the current over the shunt resistor is

$$I_{SH} = \frac{V_j}{R_{SH}} \quad 2.4$$

where

- R_{SH} is the shunt resistance (Substituting the equations (2.3, 2,4 and 2.2) into equation (2.1), we get,

$$I = I_L - I_D \left\{ \exp\left[\frac{V+IR_S}{nV_T}\right] - 1 \right\} - \frac{V+IR_S}{R_{SH}} \quad 2.5$$

The above equation is the equivalent current equation of light-generated current.

2.4.3(a) Short Circuit Current

The peak current produced when terminals are short-circuited is called the short circuit current (I_{sc}). The short circuit current is determined by the solar spectrum and the material absorption ability. The material optical characteristics determine the highest current that a solar cell can produce (e.g., absorption coefficient, bandgap and reflection coefficient) [99]. Thus, a film with a high bandgap absorbs less solar energy than one with a lower bandgap [100]. Therefore, I_{sc} rises with the reduction in the material bandgap. Equally, the J_{sc} of the cells is affected by passivating the surface and the lifetime of the minority carrier [101].

2.4.3(b) Open Circuit Voltage

The maximum voltage across the cell's terminal when current is not flowing is called an open-circuit voltage (V_{oc}). Alternative, the V_{oc} voltages is produced by forward biasing in the p-n junction when light is absorbed by the semiconducting material [102]. Thus, the more light absorbed by the material, the higher the V_{oc} [103].

Suppose that the shunt resistance is higher, then, mathematically the V_{oc} can be written as.

$$V_{oc} = \frac{nkT}{q} \text{In}\left(\frac{I_L}{I_o} - 1\right) \quad (2.6)$$

Therefore, the higher the V_{oc}, the lower the Io, since Io is inversely related to the V_{oc} and is undesirably affected by high temperatures.

2.4.3(c) Fill Factor (FF)

The fill factor (FF) is the factor that governs the determination of maximum power generated by the solar cell devices. It is calculated by taking the ratio of the maximum power output area to that of the input area [104]. Precisely, it is given by the equation.

$$FF = \frac{V_{oc}J_m}{V_{oc}J_{sc}} \quad (2.7)$$

Where J_m is the maximum current density, J_{SC} is the short circuit current density. The parameter is one of the quantities utilized for the calculation of the efficiency of the solar cell. The FF provides the highest power produced on the solar cells, as revealed by the following relation.

$$P_{max} = V_{oc}J_{sc}FF \quad (2.8)$$

Alternatively, the FF can be determined by taking the square of the I-V curve. Nevertheless, the I-V square is impossible, and some losses decrease its value [105].

2.4.3(d) Solar Cell Efficiency (η)

The percentage efficiency of solar cells is normally determined by taking the power output ratio to that of power input [106]. It is among the parameters mainly applied to determine solar cell performance. Other factors like solar intensity and temperature are also used to estimate the value of cells efficiency [107]. Thus, solar cell efficiencies are effectively measured under standard test conditions (STC), given as 25 ºC, 1000 W/m^2 irradiation and AM of 1.5 light.

The equation representing solar cell efficiency can be written as.

$$\eta = \frac{V_{oc} J_{sc} FF}{P_{in}} \tag{2.9}$$

The J_{sc} of the solar cell usually decreases with the increase in the bandgap, while the V_{oc} is increasing with the increase in the bandgap [108]. Hence there should be an ideal bandgap for solar cell efficiency to be maximum. A low J_{sc} maybe produced by losses encountered by reflection at the front of the device.

2.4.4 Diode Parameters of Solar Cells

The cell performance mainly depends on the parameters of the diode at a specific illumination intensity and temperature. The four parameters described solar cells diodes are; barrier height (Φ_B), ideality factor (η), series resistance(Ω), shunt resistance (Rs) and reverse saturation current (J) [109]. Various systematic procedures have been established for the evaluation of these parameters.

2.4.4(a) Barrier Height

A barrier height is a potential energy barrier for holes or electrons located at the metal-semiconductor junction. The value of Φ_B depends on the properties of the semiconducting materials and the combination of the metal with the semiconductor. Perhaps some metal semiconducting junction cannot create barrier height. When the metal-semiconductor allows the flow of current in both directions, which means the barrier is very low, the junction is called ohmic contact. The electrical conductivity of n-type doped semiconducting materials is due to the electrons close to the conduction band maxima (CBM). So, the barrier height can be taken by finding the difference between the electron affinity of the semiconductor and the metalwork function. While for p-type semiconductors, the carrier conductivity could be associated with the holes near the valence band maximum (VBM). Hence, the barrier height is the difference between the electron's energy barrier and semiconductors energy bandgap.

Practically, the barrier height is determined by thermionic emission (TE) theory [110], given in equation 2.12.

$$J = J_0 \exp\left[\frac{qV}{(nk_BT)} - 1\right] \tag{2.10}$$

where q is a charge, n is the ideality factor, V is the voltage use, T is the absolute temperature, k_B is the Boltzmann constant, and J_o is the current density, which can be expressed as follow [111]

$$J_0 = AA^*T^2 \exp\left[\frac{-q\Phi_B}{k_BT}\right] \tag{2.11}$$

where Φ_B is an effective barrier height under zero-bias, A is the effective diode area measured as 5.31×10^{-3} $cm^{2,}$ and A* is an effective Richardson-constant [112, 113]. Therefore the Φ_B value can be determined using the following equation:

$$\Phi_B = \left(\frac{k_B T}{q}\right) \mathrm{In}\left[\frac{AA^* T^2}{J_0}\right] \quad (2.12)$$

2.4.4(b) Ideality Factor

Ideality factor is one of the diode parameters that relate the depletion layers with the barrier height as a function of applied voltage. A perfect ideality factor is predicted theoretically to be 1. However, due to the recombination around the space-charge area, the ideality factor (n) is regulated by the properties of J_o and therefore, the ideality factor can change to a higher number like n ≈ 2. Also, the existence of the Schottky barrier in heterojunction structure makes the ideality factor higher than 2. However, the ideality factor can be determined using the thermionic emission (TE) theory given in equation 2.13.

$$\mathrm{n} = \frac{q}{(K_B T)}\left[\frac{\mathrm{d}V}{\mathrm{d}(\mathrm{In}J)}\right] \quad (2.13)$$

2.4.4(c) Series Resistance

The total resistance component along the path of the generated current in the cell is called series resistance. The series resistance is usually comprised of; the base and emitter's resistance, the metal-semiconductor contact resistance, and the metal contact resistance. The series resistance real effect is to decrease the FF values. For solar cells to be ideal, the series resistance must be small, near zero. The simplest technique to evaluate the solar cells series resistance is to use the IV curve slope at the

open-circuit voltage. The series resistance is a nearly straight-line graph. Fig. 2.6 show the impact of series resistance on the solar cell I-V characteristics.

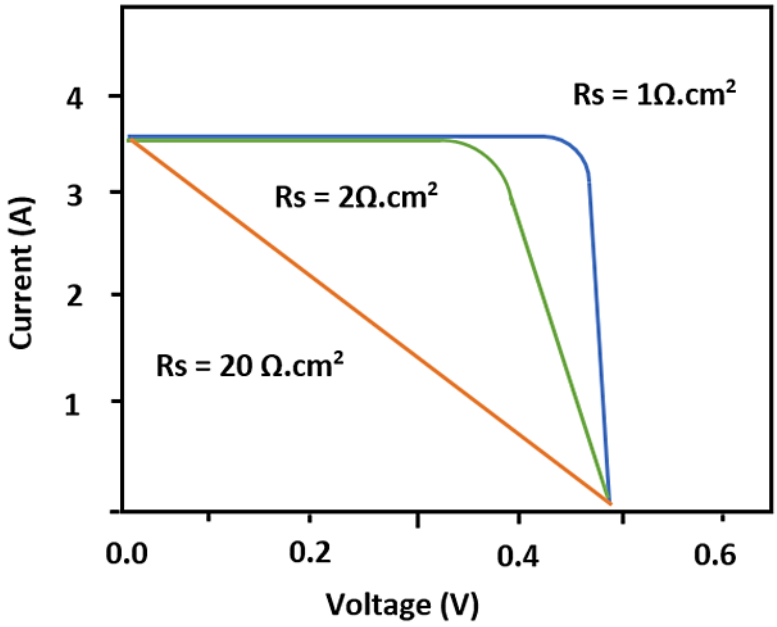

Figure 2.6: Effect of series resistance on the I-V characteristics of solar cell

2.4.4(d) Shunt Resistance

Shunt resistance, sometimes called parallel resistance, occurred due to a leakage current over the edge of the cell at different contacts polarity. When the shunt resistance is low, power losses occur in the solar cell, which provides another current route for the produced light current. The effect of shunt resistance can be seen from the IV curve, as shown in Fig. 2.7.